Chinese Chemical Letters 32 (2021) 3591–3595

Contents lists available at ScienceDirect

Chinese Chemical Letters

journal homepage: www.elsevier.com/locate/cclet

Communication

Engineering heterostructure and crystallinity of Ru/RuS_2 nanoparticle composited with N-doped graphene as electrocatalysts for alkaline hydrogen evolution

Xuyun Gao[a,b,1], Bo Li[a,1], Xuzhuo Sun[a,*], Baofan Wu[a], Yanping Hu[b], Zhichao Ning[a], Jun Li[b,*], Ning Wang[b,*]

[a] College of Chemistry and Chemical Engineering, Henan University of Technology, Zhengzhou 450001, China
[b] Key Laboratory of Synthetic and Natural Functional Molecule of the Ministry of Education, College of Chemistry & Materials Science, Northwest University, Xi'an 710069, China

ARTICLE INFO

Article history:
Received 20 February 2021
Received in revised form 19 March 2021
Accepted 22 March 2021
Available online 23 March 2021

Keywords:
Low crystallinity
Ru/RuS_2 heterostructure
Graphene
Electrocatalytic hydrogen evolution
Alkaline solution

ABSTRACT

Crystalline engineering and heterostructure have attracted much attention as effective strategies to improve the electrocatalytic activity for hydrogen evolution reaction (HER). In this study, a new heterostructure catalyst (Ru/RuS_2@N-rGO) with low crystallinity was fabricated by a simple and low-temperature method for HER in alkaline solution, applying the Na_2SO_4 as S source and polypyrrole as N source. Optimizing through the controllable crystalline engineering and composition ratio of Ru and RuS_2, the Ru/RuS_2@N-rGO heterocatalyst at the calcining 500 °C revealed highly efficient HER activity with overpotential 18 mV at a current density 10 mA/cm^2 and remarkable stability for 24 h in 1.0 mol/L KOH. This work provides a facile and effective method in designing advanced electrocatalysts for HER in the alkaline electrolytes by synergistically structural and component modulations.

Hydrogen energy has attracted much attention because of its high calorific value, rich reserves and zero CO_2 emissions, which is regarded as the most promising clean energy [1–5]. Electrocatalytic water splitting, as a significant approach for hydrogen production, has revealed broad application prospects in energy storage and conversion [6–11]. Hydrogen evolution reaction (HER) as a one-half reaction of electrocatalytic water splitting can happen in both acidic and alkaline media. However, the HER in alkaline solution suffers from relatively slow kinetics compared to that in acidic solution, thus requiring a high overpotential to drive the reaction [12–14]. The sluggish reaction rate of the HER in alkaline solution originates from the initial water dissociation step that provides protons for the subsequent reactions, but this step does not occur in acidic solution [15–17]. So, the exploration of novel electrocatalysts with high catalytic activity in alkaline solution is undertaking of great significance for reducing energy consumption.

Heterostructure [14,17–22], with double or multiple types of the active components, revealed remarkable advantages for HER, which can effectively modify the electron structure of catalytic sites. As a potential HER electrocatalyst, ruthenium (Ru) [23–25] shows higher HER performance in alkaline media than that of Pt/C, attributed to its lower energy barrier for breaking the H—OH bond [26–31]. Zheng *et al.* demonstrated the energy barriers of water dissociation were 0.41 eV and 0.51 eV for Ru_{fcc} and Ru_{hcp}, respectively, which were much lower than that of Pt ($\Delta G_B = 0.94$ eV) [26]. Ye *et al.* reported that the alkaline HER activity of RuNCs/BNG surpassed that of Pt/C, even though the intrinsic activity of Ru was inferior to that of Pt, which revealed the importance of the water dissociation barrier concerning the alkaline HER activity [32]. As we know, H adsorption/ desorption steps also play an important role in HER kinetics. The moderate M—H bond energy can balance the H-adsorption and H-desorption on the catalyst surface, which can make both of the H-adsorption and desorption happen easily on the catalyst surface [28,33–41]. However, according to DFT computations, Ru possessed relatively strong hydrogen binding, which was not favorable for the H-desorption step [15,26,28,42]. Recently, ruthenium disulfide (RuS_2) has been served as HER catalyst and exhibited moderate electrocatalytic performance, due to the Pt-similar

* Corresponding authors.
E-mail addresses: sunxuzhuo@haut.edu.cn (X. Sun), junli@nwu.edu.cn (J. Li), ningwang@nwu.edu.cn (N. Wang).
[1] These authors contributed equally to this work.

https://doi.org/10.1016/j.cclet.2021.03.053
1001-8417/

adsorption free energy of hydrogen intermediate H* [40,43–47]. Li *et al*. reported amorphous RuS_x nanoparticles supported on sulfur-doped graphene oxide (RuS_x/S—GO) required a small over-potential for acidic, neutral, alkaline solution, especially in acidic media (η_{10} = 31 mV) [43]. Zhu *et al*. reported that pyrite-type RuS_2 NPs, exhibited a significant electrocatalytic performance for the HER (η_{10} = 78 mV) in 1.0 mol/L KOH [46]. Thus, the coupling of the two components Ru and RuS_2 formed the heterostructure for HER in alkaline solution, it may be desirable for the optimization of energetics for both water dissociation and hydrogen adsorption.

Besides the intrinsic activity of the catalysts, the number of active sites is also the critical factor for catalytic performance. Low crystalline materials featuring less structural ordering can generate more active unsaturated atoms in the disordered or defect structure, which provides the opportunity to increase the number of active sites [48–51]. Sun *et al*. reported poor crystalline MoS_2/C hollow nanosphere with highly exposed active sites was rationally designed for the enhanced HER performance and long-term durability [52]. Many efforts have been made to fabricate the disordered or defect structure of MoS_2 to improve the electrocatalytic performance [52–57]. However, to the best of our knowledge, optimizing controllable crystalline engineering for Ru-based electrocatalysts has not yet been reported.

Inspired by the above viewpoints, herein we report a low crystalline catalyst Ru and RuS_2 embedded into N doped graphene (Ru/RuS_2@N-rGO) for highly efficient electrocatalytic HER in alkaline condition, which was fabricated through a simple and low-temperature method and applied the Na_2SO_4 as S sources and polypyrrole (ppy) as N source. The effect of the low crystallinity and the composition ratio of Ru and RuS_2 on the hydrogen evolution performance were discussed.

Scheme 1 revealed the synthesis route of Ru/RuS_2@N-rGO. First, the aerogels composed of 5 mg $RuCl_3$, 5 mg ppy, 20 mg GO and various quantities Na_2SO_4 were prepared as intermediate *via* ultrasonic dispersion and freeze-drying. Subsequently, the aerogels were annealed under an N_2 atmosphere at various temperatures (400−700 °C) to produce Ru/RuS_2@N-rGO. For comparison, Ru@N-rGO and Ru/RuS_2@N-rGO-x were also prepared as reference samples by adjusting the amount of Na_2SO_4 (0 mg, 2.5 mg, 10 mg and 20 mg).

The low crystallinity of synthesized catalysts depends on the calcining temperature, evolving from high crystallinity to low crystallinity with the temperature decreasing. As shown in Fig. 1a, Ru/RuS_2@N-rGO at various calcining temperatures were discussed by the powder X-ray diffraction (XRD). At 700 °C, it showed two sets of obvious and sharp peaks corresponding to Ru (PDF#06−0663) and RuS_2 (PDF#79−0618), which meant the co-existence of crystalline Ru and RuS_2 in the catalyst. Moreover, there was a broad peak at 26.4°, originating from the (002) facet of graphitic carbon (PDF#41−1487). When the calcining temperature reduced to 500 °C, it revealed three peaks at about 26.4°, 31.8° and 44.0° in XRD data, corresponding to the (002) facet of graphitic carbon, the (200) facet of RuS_2 and the (101) facet of metallic Ru, respectively. The weakening and broadening of diffraction peaks indicate the lower degree of crystallinity and more disorder structures in Ru/RuS_2 catalysts [46,50,52,57]. The reference samples Ru@N-rGO and Ru/RuS_2@N-rGO-x were prepared at 500 °C, in the presence of various amounts of Na_2SO_4. As shown in Fig. S1 (Supporting information), the XRD of Ru@N-rGO also exhibit a broad peak at 44.0°. With increasing the amount of Na_2SO_4, it found the peak of RuS_2 grows up and the peak of Ru decreases in the XRD of Ru/RuS_2@N-rGO-20. After decreasing calcining temperature further to 400 °C, XRD data of Ru/RuS_2@N-rGO showed only one broad peak of graphitic carbon's (002) facet.

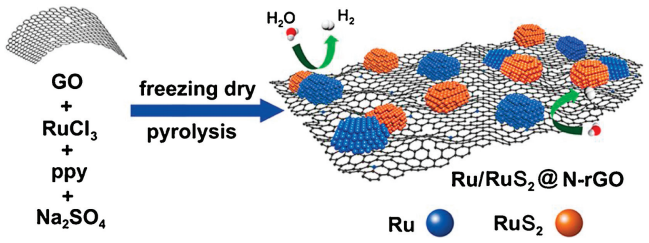

Scheme 1. Synthesis process of Ru/RuS_2@N-rGO.

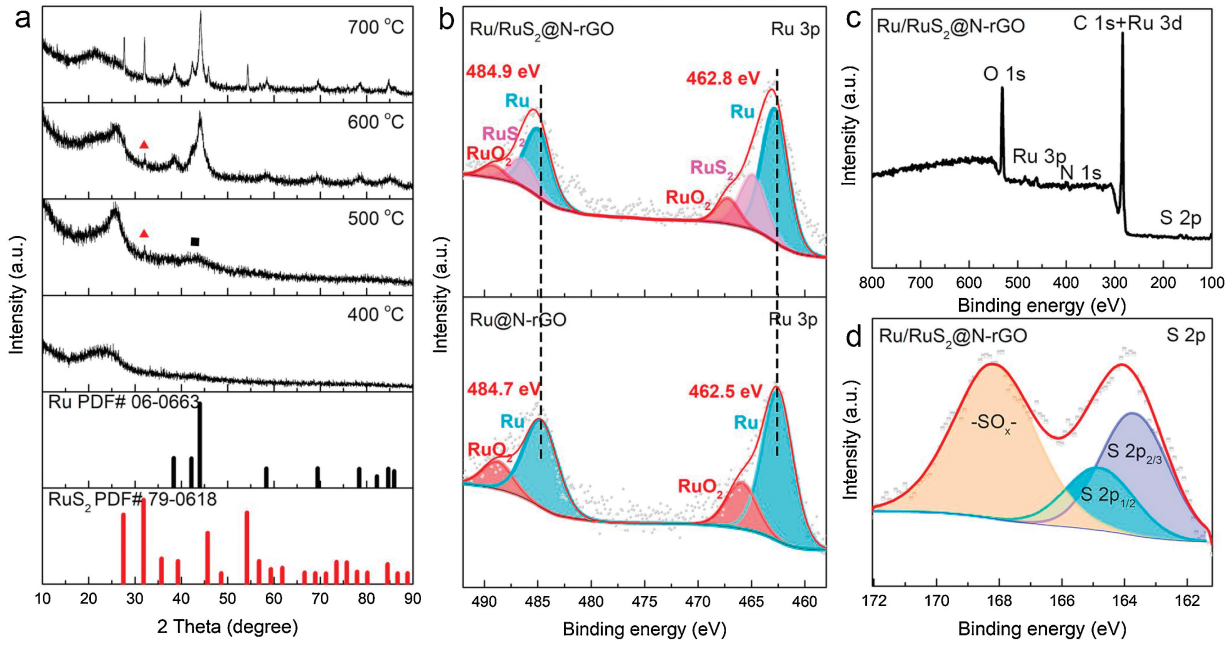

Fig. 1. (a) XRD pattern of Ru/RuS_2@N-rGO with various calcining temperatures. (b) High-resolution XPS spectra of Ru 3p of Ru/RuS_2@N-rGO and Ru@N-rGO. (c) The survey spectrum of Ru/RuS_2@N-rGO. (d) High-resolution XPS spectra of S 2p of Ru/RuS_2@N-rGO.

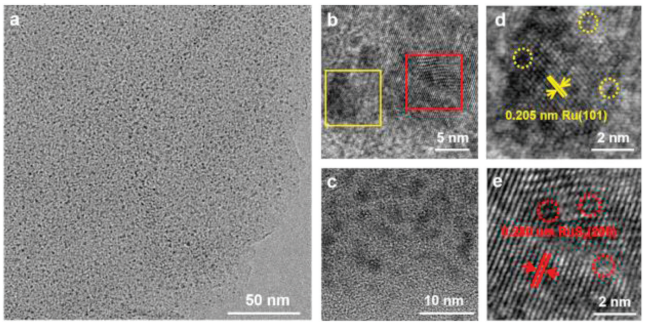

Fig. 2. (a) TEM, (b-e) HRTEM of Ru/RuS_2@N-rGO.

These indicated that the crystallinity of Ru/RuS_2 was further damaged.

The morphology of Ru/RuS_2@N-rGO at 500 °C was systematically investigated by scanning electron microscopy (SEM) and transmission electron microscopy (TEM). In the SEM image (Fig. S2a in Supporting information), it demonstrated Ru/RuS_2@N-rGO maintain the clear nanosheet structure of GO after high calcining temperature. According to energy-dispersive X-ray (EDX) elemental mapping analysis (Figs. S2b-g in Supporting information), the catalyst was revealed uniform dispersion of C, N, S, Ru in the whole nanosheet indicating the N atoms have been successfully doped into graphene. Fig. 2a presented the TEM images for Ru/RuS_2@N-rGO, in which it clearly can be observed that high-density sphere nanoparticles with an average diameter of about 3.2 nm were decorated on the surface of rGO (Fig. S3 in Supporting information). To further identify the composition of the nanoparticles, Ru/RuS_2@N-rGO was characterized with high-resolution transmission electron microscopy (HRTEM). The lattice fringe spacing of 0.205 and 0.280 nm were revealed in the HRTEM image (Figs. 2b-e), matching the D-spacing for the (101) crystallographic plane of Ru and the (200) plane of RuS_2, respectively. It further confirms the formation of Ru/RuS_2 heterostructures. Significantly, both Ru and RuS_2 lattices show lattice distortion and rich defects. And obviously discontinuous lattice fringes also appear in the lattice of RuS_2. Thus, it indicates that defect structure existed in the low crystalline Ru/RuS_2@N-rGO, which was beneficial for enhancing the catalytic activity [50].

X-ray photoelectron spectroscopy (XPS) was used to investigate the surface elemental compositions and binding states of Ru/RuS_2@N-rGO. The survey spectrum showed the presence of C, N, S and Ru (Fig. 1c), which was consistent with the EDX mapping results. The high solution XPS of N 1s of Ru/RuS_2@N-rGO confirms the doping of N atoms (Fig. S4 in Supporting information). Fig. 1b compared the high-resolution XPS spectra of Ru 3p of Ru/RuS_2@N-rGO and Ru@N-rGO. In Ru/RuS_2@N-rGO, two peaks belonged to Ru $3p_{3/2}$ (463.1 eV) and $3p_{1/2}$ (485.4 eV) were found, which could be further fitted to triplets. An apparent couple peaks centered at 462.8 eV and 484.9 eV corresponding to Ru $3p_{1/2}$ and $3p_{3/2}$, which were assigned to Ru° [19]. Another set of characteristic peaks of RuS_2 centered at 464.8 eV and 486.4 eV were observed [43]. Therefore, the coexistence of Ru and RuS_2 in Ru/RuS_2@N-rGO can be proven. For comparison, Ru 3p peaks of the sample Ru@N-rGO ascribed to Ru° obviously downshifted to 462.5 and 484.7 eV. It meant that forming the Ru/RuS_2 heterostructure can result in an obvious the electron transfer from Ru to RuS_2, which can prove that the interaction exists between metal Ru and RuS_2. In the catalysts Ru/RuS_2@N-rGO and Ru@N-rGO, each had one set of doublet peaks fitting at the higher binding energy, which were ascribed as Ru—O bond, presumably owing to surface oxidation by the exposure in the air. Compared Ru 3p spectrum of Ru/RuS_2@N-rGO and Ru/RuS_2@N-rGO-10 in Fig. S5 (Supporting information), it revealed

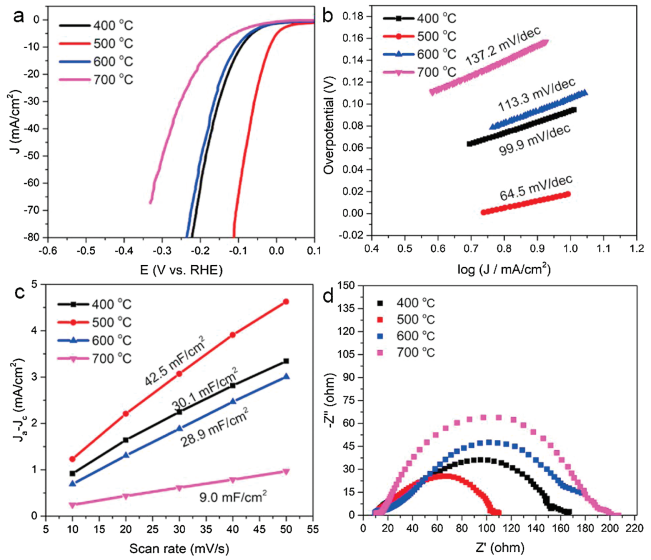

Fig. 3. HER performance for Ru/RuS_2@N-rGO annealed at various temperatures in 1.0 mol/L KOH solution. (a) Polarization curves; (b) Corresponding Tafel plots; (c, d) C_{dl} and EIS.

that the Ru 3p peaks moved to a higher region with increasing the amount of Na_2SO_4, indicating a higher valence state of Ru and higher content of RuS_2, which was consistent with the content ratio of Ru and S (Table S1 in Supporting information). The sulfur species were determined from the high resolution XPS spectrum at the S 2p region (Fig. 1d). The S 2p XPS spectra revealed that the binding states of sulfur were $2p_{3/2}$ (163.7 eV), $2p_{1/2}$ (164.8 eV) and -C-SO_x peak (168.1 eV). The doublet at binding energies of 163.7 and 164.8 eV corresponded to the S $2p_{3/2}$ and S $2p_{1/2}$ of the Ru—S bond, respectively. It further indicated the existence of RuS_2.

In order to determine the effects of the degree of crystallinity and the heterostructure of Ru/RuS_2 on the electrocatalytic HER activity, the relevant electrocatalytic tests were systematically studied using a typical three-electrode electrochemical system in Ar-saturated 1.0 mol/L KOH. For comparison, that of the commercial Pt/C (20 wt%) catalyst was also measured under the same conditions. The electrocatalytic HER performance of Ru/RuS_2@N-rGO annealed at various temperatures were displayed in Fig. 3a. The HER activity of Ru/RuS_2@N-rGO varies with the annealing temperature obviously. As the temperature drops from 700 °C to 500 °C, the activity of the catalyst is significantly improved. Noticeably, the sample calcined at 500 °C exhibits the highest catalytic activity towards HER, only 18 mV to reach 10 mA/cm^2, which is much lower than Ru/RuS_2@N-rGO-700 (161 mV), Ru/RuS_2@N-rGO-600 (132 mV) and Ru/RuS_2@N-rGO-400 (93 mV). It suggests the low crystalline structure can greatly improve the HER activity. As shown in Table S2 (Supporting information), it found that the overpotential of Ru/RuS_2@N-rGO is superior to that of Pt/C and comparable with most of the reported electrocatalysts. The HER kinetics behavior of the catalyst was evaluated by the Tafel slope, which showed that the catalyst exhibited the fastest kinetic process at a lower crystallinity (500 °C) (Fig. 3b). In addition, electrochemically active surface area (ECSA) is a vital factor in determining the HER activity, which was evaluated by double-layer capacitance (C_{dl}) based on the cyclic voltammograms at different scan rates. In Fig. 3c, Ru/RuS_2@N-rGO catalyst had the highest C_{dl} value of 42.5 mF/cm^2, which was nearly 5 times as much as that of Ru/RuS_2@N-rGO at 700 °C. It can clearly prove that a low crystalline structure can expose more active sites. The Ru/RuS_2@N-rGO also reveals the smallest R_{ct}, suggesting ultrafast interface electron transfer rate and high conductivity (Fig. 3d).

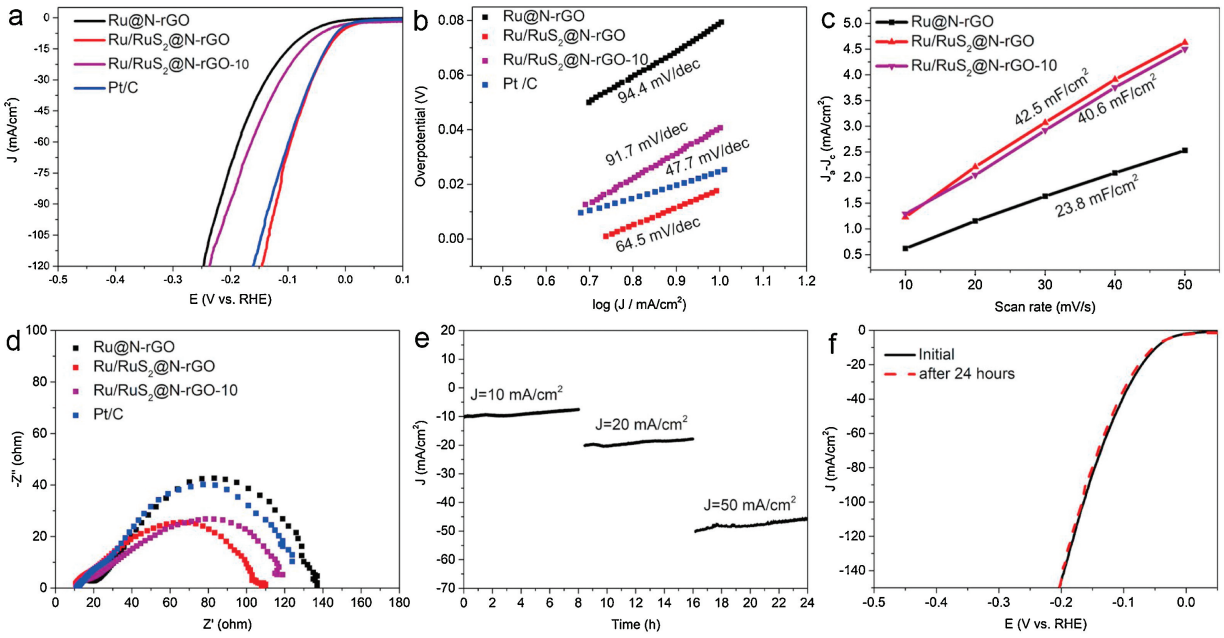

Fig. 4. HER performance in 1.0 mol/L KOH solution. (a) Polarization curves; (b) Corresponding Tafel plots; (c, d) Cdl and EIS for Ru/RuS_2@N-rGO with various Na_2SO_4 salts, Ru@N-rGO and Pt/C; (e) Chronoamperometric curve operated at a fixed current density of 10, 20 and 50 mA/cm^2; (f) LSV curves for Ru/RuS_2@N-rGO before and after the chronoamperometric test of 24 h.

According to the results above, it was suggested that low crystallinity can greatly improve HER activity, which was more likely to attribute to increasing the number of active sites.

As shown in Fig. 4a, Ru/RuS_2@N-rGO exhibited higher catalytic activity than that of Ru@N-rGO (79 mV), Ru/RuS_2@N-rGO-10 (55 mV), and commercial Pt/C (25 mV). This finding indicated that introducing RuS_2 into Ru to form heterostructure can improve hydrogen evolution performance. In order to explore the reasons for excellent HER of Ru/RuS_2 heterostructure, the corresponding Tafel plots were further calculated and fitted based on the polarization curves, as shown in Fig. 4b. The Tafel slope of Ru/RuS_2@N-rGO was 64.5 mV/dec, lower than that of Ru@N-rGO (94.4 mV/dec), Ru/RuS_2@N-rGO-10 (91.7 mV/dec) and approach that of Pt/C (47.7 mV/dec), suggesting its favorable reaction kinetics. It can illustrate that Ru/RuS_2 heterostructure can boost reaction kinetics towards alkaline HER through the coupling of water dissociation on Ru and hydrogen adsorption on RuS_2. The ECSA of Ru@N-rGO and Ru/RuS_2@N-rGO with various amounts of Na_2SO_4 were evaluated by C_{dl} (Fig. S6 in Supporting information). As shown in Fig. 4c, the C_{dl} of Ru/RuS_2@N-rGO (42.5 mF/cm^2) and Ru/RuS_2@N-rGO-10 (40.6 mF/cm^2) more than two times that of Ru@N-rGO (23.8 mF/cm^2). Ru/RuS_2@N-rGO also showed a much lower charge transfer resistance in comparison with other catalysts in Fig. 4d and Fig. S7b (Supporting information), suggesting that Ru/RuS_2@N-rGO possesses excellent conductivity and the faster charge transfer. It is noticeable that the reference catalyst Ru/RuS_2@rGO without N doping had much higher charge transfer resistance, which may indicate that N doping also plays an important role in accelerating charge transfer (Fig. S7b).

The long-term electrocatalytic stability is a crucial requirement for evaluating the electrocatalyst. Fig. 4e showed the chronoamperometric curve of Ru/RuS_2@N-rGO under the potential at 10, 20 and 50 mA/cm^2, in which the current density almost kept constant over 24 h. After 24 h electrocatalytic stability test, Ru/RuS_2@N-rGO did not show an observable shift in the polarization curve, suggesting that it had superior electrochemical stability upon long-term operating (Fig. 4f). Moreover, The Ru 3p XPS peaks of the samples still maintained a similar value after the electrocatalytic test (Fig. S8 in Supporting information). As shown in Figure S9, the morphologies of Ru/RuS_2@N-rGO also have no obvious change after 24 h stability test. It indicated that Ru/RuS_2@N-rGO had superior electrochemical stability upon long-term operation.

Ru/RuS_2 heterostructure with low crystallinity has been successfully synthesized by controlling calcining temperature and adjusting the amount of Na_2SO_4. The catalyst Ru/RuS_2@N-rGO exhibited excellent HER activity and stability under alkaline media. It observed the low η_{10} of 18 mV, superior to benchmark Pt/C catalysts, and remarkable stability for 24 h. The excellent activity can be ascribed to its rationally designed composition with favorable structure morphology. Firstly, the low crystallinity can induce larger electrochemically active surface areas for exposing more active sites. Secondly, the reaction kinetics for alkaline HER are significantly improved by the heterostructural synergy between Ru and RuS_2 nanoparticles. The synergistic effect of Ru/RuS_2 heterostructure not only couples the water dissociation on Ru and hydrogen adsorption on RuS_2, but also modifies the electron structure and further improves the chemisorption of the different reaction intermediates. Besides, the defect was beneficial for enhancing the catalytic performance. This work provides a new and facile way for improving catalytic activity through synergistically structural and component modulations.

Declaration of competing interest

The authors report no declarations of interest.

Acknowledgments

This work was supported by National Natural Science Foundation of China (Nos. 21773184 and 21671158), Key Science and Technology Project of Henan (No. 202102210238), Natural Science Foundation of Henan (No. 212300410339) and Cultivation Program for Young Backbone Teachers in Henan University of Technology (Nos. 21420108 and 21420073).

Appendix A. Supplementary data

Supplementary material related to this article can be found, in the online version, at doi:https://doi.org/10.1016/j.cclet.2021.03.053.

References

[1] S. Chu, A. Majumdar, Nature 488 (2012) 294–303.
[2] J.A. Turner, Science 305 (2004) 972–974.
[3] Y.F. Yu, Y.M. Shi, B. Zhang, Acc. Chem. Res. 51 (2018) 1711–1721.
[4] X. Wang, Q.X. Li, P.H. Shi, et al., Small 15 (2019) 1901530.
[5] X. Ding, L.L. Zhang, Y. Wang, A.H. Liu, Y. Gao, Coord. Chem. Rev. 357 (2018) 130–143.
[6] T. Liu, P. Li, N. Yao, et al., Angew. Chem. Int. Ed. 58 (2019) 4679–4684.
[7] G. Huang, Z.H. Xiao, R. Chen, S.G. Wang, ACS Sustain. Chem. Eng. 6 (2018) 15954–15969.
[8] Y. Jiao, Y. Zheng, M. Jaroniec, S.Z. Qiao, Chem. Soc. Rev. 44 (2015) 2060–2086.
[9] K.D. Xia, J.P. Guo, C.J. Xuan, T. Huang, Z.P. Deng, Chin. Chem. Lett. 30 (2020) 192–196.
[10] Y.M. Zhao, H.J. Cong, W. Luo, et al., Angew. Chem. Int. Ed. 60 (2021) 1–6.
[11] K.D. Li, J.F. Zhang, R. Wu, Y.F. Yu, B. Zhang, Adv. Sci. 3 (2016) 1500426.
[12] N. Mahmood, Y.D. Yao, J.W. Zhang, et al., Adv. Sci. 5 (2018) 1700464.
[13] F. Safizadeh, E. Ghali, G. Houlachi, Int. J. Hydrogen Energy 40 (2015) 256–274.
[14] J.M. Wei, M. Zhou, A.C. Long, et al., Nano-micro Lett. 10 (2018) 75.
[15] J.L. Liu, Y. Zheng, D.D. Zhu, et al., Nanoscale 9 (2017) 16616–16621.
[16] B.Y. Lu, L. Guo, F. Wu, et al., Nat. Commun. 10 (2019) 631.
[17] R. Subbaraman, D. Tripkovic, D. Strmcnik, et al., Science 334 (2011) 1256–1260.
[18] R. Boppella, J.W. Tan, W. Yang, J. Moon, Adv. Funct. Mater. 29 (2018) 1807976.
[19] X.Y. Gao, J. Chen, X.Z. Sun, et al., ACS Appl. Nano Mater. 3 (2020) 12269–12277.
[20] Z.J. Sun, Y. Liang, Y.M. Wu, Y.F. Yu, B. Zhang, ACS Sustain. Chem. Eng. 6 (2018) 11206–11210.
[21] J.X. Diao, Y. Qiu, S.Q. Liu, et al., Adv. Mater. 32 (2019) 905679.
[22] X.L. Jiang, H. Jang, S.G. Liu, et al., Angew. Chem.Int. Ed. 60 (2021) 4110–4116.
[23] S. Higgins, Nat. Chem. 2 (2010) 1100-1100.
[24] Y.T. Li, L.A. Zhang, Y. Qin, et al., ACS Catal. 8 (2018) 5714–5720.
[25] J. Yu, Q.J. He, G.M. Yang, et al., ACS Catal. 9 (2019) 9973–10011.
[26] Y. Zheng, Y. Jiao, Y.H. Zhu, et al., J. Am. Chem. Soc. 138 (2016) 16174–16181.
[27] W.D. Li, Y.A. Liu, M. Wu, et al., Adv. Mater. 30 (2018) 1800676.
[28] J.W. Liu, G.Z. Ding, J.Y. Yu, et al., J. Mater. Chem. A Mater. Energy Sustain. 7 (2019) 18072–18080.
[29] Z.K. Peng, H.Y. Wang, L.L. Zhou, et al., J. Mater. Chem. A Mater. Energy Sustain. 7 (2019) 6676–6685.
[30] X.Z. Sun, X.Y. Gao, J. Chen, et al., ACS Appl. Mater. Interfaces 12 (2020) 48591–48597.
[31] M. Tan, Y. Wang, A. Taguchi, et al., Int. J. Hydrogen Energy 44 (2019) 7320–7325.
[32] S.H. Ye, F.Y. Luo, T.T. Xu, et al., Nano Energy 68 (2020) 104301.
[33] X.L. Chen, J. Zheng, X. Zhong, et al., Catal. Sci. Technol. 7 (2017) 4964–4970.
[34] W.Y. Gou, J.Y. Li, W. Gao, et al., ChemCatChem 11 (2019) 1970–1976.
[35] X.K. Kong, K. Xu, C.G. Zhang, et al., ACS Catal. 6 (2016) 1487–1492.
[36] D. Luo, B.Y. Zhou, Z.X. Li, et al., J. Mater. Chem. A Mater. Energy Sustain. 6 (2018) 2311–2317.
[37] W. Luo, L.B. Li, N. Yao, F.L. Yang, G.Z. Cheng, ACS Catal. 10 (2020) 73322–77327.
[38] Y. Peng, B.Z. Lu, L.M. Chen, et al., J. Mater. Chem. A Mater. Energy Sustain. 5 (2017) 18261–18269.
[39] J. Wang, Z.Z. Wei, S.J. Mao, H.R. Li, Y. Wang, Energy Environ. Sci. 11 (2018) 800–806.
[40] J. Yu, Y.N. Guo, S.S. Miao, et al., ACS Appl. Mater. Interfaces 10 (2018) 34098–34107.
[41] J.Y. Yu, Y.S. Yang, R.T. Jia, et al., Appl. Surf. Sci. 529 (2020) 147080.
[42] U. Joshi, S. Malkhandi, Y. Ren, et al., ACS Appl. Mater. Interfaces 10 (2018) 6354–6360.
[43] P.S. Li, X.X. Duan, S.Y. Wang, et al., Small 15 (2019) 1904043.
[44] Y. Li, J.W. Li, J.X. Chen, et al., J. Power Sources 472 (2020) 228625.
[45] Y.J. Xia, W.Q. Wu, H. Wang, et al., Nanotechnology 31 (2020) 145401.
[46] Y.L. Zhu, H.A. Tahini, Y. Wang, et al., J. Mater. Chem. A Mater. Energy Sustain. 7 (2019) 14222–14232.
[47] J.W. Zhu, Y. Guo, F. Liu, et al., Angew. Chem. Int. Ed. 60 (2021) 12328-12334.
[48] Y.P. Li, Y.F. Yu, Y.F. Huang, et al., ACS Catal. 5 (2014) 448–455.
[49] M. Zhao, Y.F. Wu, W.W. Cai, et al., Int. J. Hydrogen Energy 44 (2019) 31053–31061.
[50] X.Y. Zhang, T. Guo, T.Y. Liu, et al., Electrochim. Acta 323 (2019) 134798.
[51] C. Zhang, Y.M. Shi, Y.F. Yu, Y.H. Yu, B. Zhang, ACS Catal. 8 (2018) 8077–8083.
[52] H.H. Sun, X.Y. Ji, Y.F. Qiu, et al., J. Alloys. Compd. 777 (2019) 514–523.
[53] J. Kibsgaard, Z.B. Chen, B.N. Reinecke, T.F. Jaramillo, Nat. Mater. 11 (2012) 963–969.
[54] C. Sun, P.P. Wang, H. Wang, et al., Nano Res. 12 (2019) 1613–1618.
[55] H. Wang, X. Xiao, S.Y. Liu, et al., J. Am. Chem. Soc. 141 (2019) 18578–18584.
[56] X. Wang, Y.W. Zhang, H.N. Si, et al., J. Am. Chem. Soc. 142 (2020) 4298–4308.
[57] J.F. Xie, J.J. Zhang, S. Li, et al., J. Am. Chem. Soc. 135 (2013) 17881–17888.